Toll-Like Receptor 2 Promotes Breast Cancer Progression and Resistance to Chemotherapy

Antonino Di Lorenzo
University of Turin: Universita degli Studi di Torino
Elisabetta Bolli
University of Turin: Universita degli Studi di Torino
Roberto Ruiu
University of Turin: Universita degli Studi di Torino
Giuseppe Ferrauto
University of Turin: Universita degli Studi di Torino
Enza Di Gregorio
University of Turin: Universita degli Studi di Torino
Lidia Avalle
University of Turin: Universita degli Studi di Torino
Irene Fiore Merighi
University of Turin: Universita degli Studi di Torino
Federica Riccardo
University of Turin: Universita degli Studi di Torino
Elena Quaglino
University of Turin: Universita degli Studi di Torino
Federica Cavallo
University of Turin: Universita degli Studi di Torino
Laura Conti (laura.conti@unito.it)
University of Turin: Universita degli Studi di Torino https://orcid.org/0000-0003-1780-098X

Research Article

Keywords: Breast Cancer, Toll-Like Receptor 2, HER2, HMGB1, chemoresistance

Posted Date: November 1st, 2021

DOI: https://doi.org/10.21203/rs.3.rs-1015076/v1

Version of Record: A version of this preprint was published at OncoImmunology on June 15th, 2022. See the published version at https://doi.org/10.1080/2162402X.2022.2086752.

Abstract

Background. Breast cancer (BC) is the leading cause of cancer death in women, due to the development of resistance to current therapies, including chemotherapy. Since breast cancer stem cells (CSCs) are the main drivers of therapy resistance and disease progression, chemoresistance might be prevented targeting the molecules that promote their self-renewal. We previously demonstrated that Toll-like Receptor (TLR)2 is overexpressed in CSCs, which exploit it to promote their self-renewal through an autocrine loop initiated by high mobility group box (HMGB)1. TLR2 expression in BC is associated with poor prognosis in patients, suggesting that it could be a good target for BC therapies.

Methods. We generated and characterized $TLR2^{WT}$ and $TLR2^{KO}$ autochthonous mammary cancer mouse models. *In-vitro* and *in-vivo* studies were performed to assess the efficacy of TLR2 silencing and inhibition in combination with chemotherapy.

Results. $TLR2^{KO}$ mice displayed delayed tumor onset, increased survival, and reductions in CSC and T regulatory cell frequency, compared to $TLR2^{WT}$ mice. Transplantation experiments using $TLR2^{WT}$ and $TLR2^{KO}$ cells injected subcutaneously into $TLR2^{WT}$ and $TLR2^{KO}$ mice showed that TLR2 mainly acts via cancer-cell-intrinsic mechanisms, such as increased cell survival and CSC self-renewal. Moreover, TLR2 promoted cancer cell resistance to chemotherapy following the doxorubicin-induced release of HMGB1. Thus, TLR2 inhibitors impaired the viability and induced the apoptosis of BC cells and exerted a synergistic effect when administered with chemotherapy both *in-vitro* and *in-vivo*.

Conclusions. We have demonstrated that TLR2 inhibitors reinstate BC response to chemotherapy, opening new perspectives for the treatment of BC patients.

Background

Breast cancer (BC) is the most prevalent cancer in women, and its incidence is progressively increasing [1]. Remarkable advances in diagnosis and adjuvant and neoadjuvant treatments have improved patient outcomes. However, BC is still the first cause of cancer-associated mortality in women in more than 100 countries [1]. More than 30% of patients experience local or distal relapse after surgery, and about 80% of deaths occur in patients whose BC progressed to metastatic disease despite treatment [2].

Although endocrine and HER2-targeted therapies are commonly used for estrogen receptor (ER)- and HER2-positive early BCs, respectively, systemic chemotherapy with anthracyclines or cyclophosphamide is the cornerstone of treatment for triple negative (TN) BC, high-risk luminal cancers, and advanced BC. Neoadjuvant chemotherapy using a doxorubicin-based schedule has recently become a common therapeutic option for operable BC [3]. However, the emergence of chemoresistance is a common event that often leads to treatment failure and metastasis [4].

Resistance to chemotherapy can be attributed to several cancer-cell-intrinsic mechanisms, including altered drug absorption, efflux or metabolism, the increased activation of pro-survival pathways,

enhanced DNA repair and tumor stemness [4]. Furthermore, chemotherapy induces alterations in several cells that are present in the tumor microenvironment (TME), and tumor cells exploit these alterations to stimulate their survival and proliferation, resulting in cancer progression [4, 5]. One of these mechanisms is mediated by damage-associated molecular patterns (DAMPs), which are a wide-ranging group of biomolecules released from damaged or dying cells and which interact with pattern recognition receptors (PRRs). Physiologically, PRRs are expressed on immune cells and promote inflammatory responses [6]. However, several PRRs have recently been observed on cancer cells as well, where they can activate pro-tumor pathways, and thus act as a double-edge sword in cancer [6, 7].

We have previously demonstrated that BC cells express Toll-like receptor (TLR)2, a PRR that plays a key role in the survival and self-renewal of cancer stem cells (CSCs), which are a small population of chemoresistant cancer cells that are responsible for tumor relapse and metastasis [8]. TLR2 activation in breast CSCs is autocrinally induced by the secretion of the DAMP High Mobility Group Box (HMGB)1, and leads to the activation of the NF-κB, AKT and MAPK pathways and the subsequent production of Interleukin (IL)-6, tumor growth factor (TGF)-β, granulocytic-colony stimulating factor (G-CSF), and vascular endothelial growth factor (VEGF) [6, 8]. These cytokines induce STAT3- and Smad3-pathway activation, promoting CSC survival, proliferation, self-renewal, and invasion [8].

Besides being actively secreted by CSCs [8], HMGB1 can be released into the TME as a consequence of treatment with chemotherapeutic drugs, including doxorubicin and taxanes, that induce immunogenic cell death [9]. High HMGB1 levels have been associated with clinical progressive disease during neoadjuvant chemotherapy in TNBC patients [10]. Based on this evidence, we hypothesize that HMGB1 released in chemotherapy-treated tumors may activate TLR2 and promote BC progression. Thus, TLR2 inhibition may synergize with chemotherapy.

Herein, we show that TLR2 promotes BC growth and chemoresistance, mainly via tumor cell-intrinsic mechanisms, and that its inhibition improves the efficacy of doxorubicin in preclinical models of BC. This study therefore identifies TLR2 as a new potential target for combined therapies.

Materials And Methods

Cell cultures

MDA-MB-231 and 4T1 were purchased from the American Type Culture Collection (ATCC) in 2018, aliquoted, frozen, and then used within 10 passages after resuscitation in DMEM or RPMI 1640 (ThermoFisher Scientific) 10% FBS (Sigma-Aldrich), respectively. TUBO were derived from a BALB-neuT primary tumor and cultured in DMEM 20% FBS [11]. The WT874, KO-M26 and KO-E26 cell lines were derived, as described in [12], from mammary tumors isolated from C57Bl6-neuT mice either TLR2 wild-type (neuT-TLR2^{WT}) or TLR2-Knock-out (neuT-TLR2^{KO}), respectively, and cultured in DMEM-F12 (ThermoFisher Scientific) 20% FBS. All cells were negative for mycoplasma [13].

Meta-analysis using patient databases

The prognostic value of TLR2 mRNA expression in the 5-year-relapse-free (RFS) and overall survival (OS) of patients with BC, either treated with chemotherapy or not, was analyzed using the GSE1456 [14], GSE4611, GSE6532, GSE19615, GSE20711, GSE25066 and GSE42568 datasets, and the open access online software Kaplan-Meier Plotter [15, 16]. Patients were stratified into two groups according to TLR2 expression using the “auto select best cutoff” function. The removal of redundant samples, the exclusion of biased arrays and the proportional hazard assumptions check were included in quality control. The TLR2 mRNA expression levels in BC patients that responded to adjuvant chemotherapy and those that did not were analyzed using the datasets and tools available [17, 18]; patients who relapsed within five years of treatment were compared with patients who did not, excluding those censored before the five years had passed.

Mice

Mice were bred and maintained under saprophytic and pathogen-free conditions at the animal facility of the Molecular Biotechnology Center, and treated in accordance with EU and institutional guidelines, with the approval of the Animal Care and Use Committee of the University of Turin and the Italian Ministry of Health (authorizations N° 107/2020-PR and 500/2017-PR).

neuT-TLR2^{WT} mice were generated by crossing male BALB-neuT [11] with C57Bl6 female mice, and then backcrossing neuT male offspring with C57Bl6 mice for 12 generations. neuT-TLR2^{WT} male mice were then crossed with B6.129-*Tlr2*^{tm1Kir}/J female mice (The Jackson Laboratory), and the *Tlr2*^{Het} offspring intercrossed to obtain neuT-TLR2^{KO} mice. Mice were screened with primers to *NeuT* (Fwd:5’-GTAACACAGGCAGATGTAGGA-3’; Rev:5’-ATCGGTGATGTCGGCGATAT-3’), *Tlr2* (Fwd:5’-CTTCCTGAATTTGTCCAGTACA-3’; RevWT:5’-GGGCCAGCTCATTCCTCCCAC-3’; Rev *Tlr2*^{tm1Kir}5’-GAAACGGAATGTTGTGGAGT-3’) and *b-casein* (Fwd:5’-GATGTGCTCCAGGCTAAAGTT-3’; Rev:5’-AGAAACGGAATGTTGTGGAGT-3’), according to Jackson Laboratory website protocols. Tumor growth was monitored twice per week with a caliper (N=20 per group) until all 10 mammary glands displayed a tumor, or a tumor that exceeded 10 mm mean diameter.

1x10^6 WT-874, KO-E26 and KO-M26 cells were injected orthotopically into the fourth mammary gland of 8-week-old syngeneic C57Bl6 mice either TLR2^{WT} or TLR2^{KO} and NOD SCID IL-2 receptor gamma chain deficient (NSG, Charles River Laboratories) female mice (N = 6 per group). Tumor growth was monitored twice per week by caliper. All mice were culled when the WT-874 tumors reached 10 mm in mean diameter.

1x10^4 4T1 cells were transfected with a pool of TLR2-specific or scrambled siRNAs, injected orthotopically, 24 hours later, into 6-week-old female BALB/c mice (Charles River Laboratories) and tumor growth was monitored. In the therapeutic model, 1x10^4 4T1 cells were injected orthotopically into 40 6-week-old female BALB/c mice. When the tumors reached 2 mm mean diameter, the mice were blindly randomized into four groups, which received: intratumor and intraperitoneal (i.p.) injections of the vehicle (control); 50 µg CU-CPT-22 (Tocris Bioscience, Cat#4884) intratumorally and vehicle i.p. (CU-CPT-22-

treated); 3 mg/Kg doxorubicin (Sigma-Aldrich, Cat#D1515) i.p. and vehicle intratumorally (doxorubicin-treated); or 50 µg CU-CPT-22 intratumorally and 3 mg/Kg doxorubicin i.p. (CU-CPT-22 + doxorubicin-treated) twice per week. When the control tumors reached 10 mm in mean diameter, the mice were culled, the tumors removed and processed for FACS, and the lungs were fixed in 4% formaldehyde, paraffin embedded, sectioned into four sections spaced by 50 µm and H&E stained. Pictures were acquired using a Nikon SMZ1000 stereomicroscope (Mager Scientific) and the metastases counted with ImageJ [19].

Ex-vivo T regulatory cell (Treg) analysis

The blood of tumor-bearing neuT-TLR2^{WT} mice was collected and processed, and the T cells were activated as in [20], and then either treated or not, with 20 µg/ml peptidoglycan from *S. aureus* (PGN-SA; InvivoGen, Cat#tlrl-pgns2) or 10 µg/ml HMGB1 (Sigma-Aldrich, Cat#SRP6265). The percentage of Tregs was analyzed six days later by FACS.

FACS analysis

Single-cell suspensions were obtained from the fresh primary tumors, spleens, and heparinized blood as in [21]. 1x10^6 cells were treated with the Fc-receptor blocker (BD Bioscience, Cat#01245B) and stained for 20 min at 4°C with anti-mouse CD45-VioGreen (Cat#130-110-803), CD11b-FITC (Cat#130-110-803), CD3-FITC (Cat#130-119-135), CD4-APC-Vio770 (Cat#130-119-134), CD8-VioBlue (Cat#130-123-865), CD49b-PE (Cat#130-123-702), B220-PE-Vio770 (Cat#130-123-702), gd TCR-PE/Cy7 (Cat#130-123-290), Gr1-VioBlue (Cat#130-102-830), F4/80-PE-Vio770 (Cat#130-118-320) and MHC-II-APC (Cat#130-102-139) from Miltenyi Biotec, and CD44-PE (Cat#103007), CD24-PE/Cy7 (Cat#101822), Sca-1-AlexaFluor 647 (Cat#122518), CD206-PE (Cat#141706), CD4-PE/Cy7 (Cat#100528), GITR-PE (Cat#126310), TLR2-PE (Cat#148604) and CD25-APC (Cat#101910) from Biolegend, and the Aldefluor kit (Stem Cell Technologies, Cat#01700) and the anti-FoxP3-FITC staining kit (eBioscience, Cat#10191071-5775-40) [22]. At least 50,000 CD45$^+$ events were acquired per sample on a BD-FACSVerse and analyzed with FlowJO10.5.3. Cells were gated according to their physical parameters, and dead cells were excluded following propidium iodide (Sigma-Aldrich, Cat#P4864) staining. The CD45$^+$ leucocytes and CD45$^-$ cells were gated, and the cell populations were analyzed as follows: NK: CD3$^-$ CD49b$^+$; CD4$^+$ T cells: CD3$^+$ CD49b$^-$ CD4$^+$; CD8$^+$ T cells: CD3$^+$ CD49b$^-$ CD8$^+$; gd TCR$^+$ T cells: CD3$^+$ CD49b$^-$ gd TCR$^+$; Tregs: CD3$^+$ CD4$^+$ CD25^{high} GITR$^+$ Foxp3$^+$; B cells: CD3$^-$ B220$^+$; MDSC: CD11b$^+$ Gr1$^+$; M1 macrophages: CD11b$^+$ F4/80$^+$ MHC-II$^+$ CD206$^-$; M2 macrophages: and CD11b$^+$ F4/80$^+$ CD206$^+$ [23, 24]; CSC: CD45$^-$ Sca1$^+$, CD45$^-$ CD44$^+$ CD24$^-$ and CD45$^-$ Aldefluor$^+$ [21]. Tumor cells were either treated with 5 or 0.2 µM doxorubicin and/or with 5 µM CU-CPT-22 or 10 µg/ml of the HMGB1 inhibitor BOX-A (HMGBIotech Cat#HM-014) or 8 µM of the %NF-κB inhibitor BAY 11-7082 (Sigma-Aldrich, Cat#B5556) for 48 hours, or left untreated, and then stained with AnnexinV-Apoptosis Kit-APC (eBioscience, Cat#88-8007-72) [25]. To analyze NF-κB activation, cells were either treated with 5 µM doxorubicin and/or 5 µM CU-CPT-22 for 48 hours or starved in serum-free medium for 4 hours and then stimulated for 30 min with or without 10 µg/ml HMGB1. Cells were fixed with 4% formaldehyde and 90% methanol (Sigma-Aldrich), permeabilized and stained for 30

min at 4°C with Alexa Fluor647-conjugated anti-pNF-κB p65-S536 (Cell Signaling Technology, Cat#4887) [8].

3-(4,5-Dimethylthiazol-2-yl)-2,5-Diphenyltetrazolium Bromide (MTT) assay

5×10^3 cells were cultured overnight in 96-well plates, and scalar doses of either CU-CPT-22 or doxorubicin, alone or with 5 μM CU-CPT-22, were then added. Viability was measured 48 hours after by MTT (0.5 mg/ml; Sigma Aldrich, Cat#M2128) [21]. The combined effect of doxorubicin and CU-CPT-22 was determined as in [26] using Bliss independence analyses, which were calculated using the equation: C = (A + B) − (A × B), where A and B are the fractional growth inhibitions of doxorubicin at a given dose and CU-CPT-22. “Delta Bliss” scores (the difference between the observed growth inhibition and the Bliss expectation at the same dose) of the different doses were summed to generate a Bliss score. Bliss score = 0: additive effect, Bliss score > 0: synergy, Bliss score < 0: antagonism.

Tumorsphere-generation assays

Tumorspheres were generated from cell lines or cells dissociated from tumors [8]. Dissociated tumorspheres were transfected with a pool of TLR2-specific (MSS216272, MSS216273, MSS280579) or scrambled (Cat#12935110) siRNAs using Lipofectamine2000 (all from ThermoFisher Scientific). 24 hours later, cells were treated with 20 μg/ml PGN-SA or 10 μg/ml HMGB1 or left untreated. After four days, contrast phase images were acquired (10X) and the number of spheres counted (4X) using a Zeiss Axio Observer or a Leica DMi1 inverted microscope connected to a DC120 digital camera [21].

ELISA

The supernatants of cells treated with 5 μM or 0.2 μM doxorubicin or left untreated were harvested after 48 hours, and HMGB1, IL-6, TGF-b and VEGF were quantified using ELISA (IBL International GmbH, Cat#ST51011 and R&D Systems, Cat#DY406, DY1679, DY493).

Magnetic Resonance Imaging

MR images were acquired at 7.1T on a Bruker Avance300 spectrometer equipped with the Micro2.5 microimaging probe at room temperature. T_{2W} morphological images were acquired using a standard RARE (Rapid Acquisition with Refocused Echoes) sequence with the following parameters: TR=4000 ms, TE=40.57 ms, RARE factor=24, flip angle=180°, number of averages=4, FOV=30 mm x 30 mm, slice thickness 1 mm, matrix size 256x256, and spatial resolution=0.117x0.117 mm/pixel. Diffusion-Weighted MR Images (DWI-MRI) were acquired using a Spin Echo sequence with TE=27 ms, TR=750 ms, number of averages=1, FOV=30x30 mm, slice thickness=1 mm, matrix size 128x128, and spatial resolution=0.234x0.234 mm/pixel. Six different B-values were used (0, 150, 250, 500, 755 and 1000 s/mm^2). Apparent diffusion constant (ADC) maps were calculated by fitting DW-MRI signal intensity as a function of B-values using Bruker ParaVision360 software [27]. ADC maps were obtained by superimposing the ADC values of the tumor ROI onto T_{2W} MRI (Fiji- ImageJ software).

Statistical analysis

Statistical significance was evaluated using GraphPad8 software. Differences in tumor-free mice and survival were analyzed using the Mantel-Cox log-rank test. Differences in sphere formation, FACS and ELISA data, tumor multiplicity and growth were analyzed using the two-tailed unpaired Student's t-test and the non-parametric Mann-Whitney or Kruskal-Wallis test when the distribution calculated using the Shapiro-Wilk or Kolmogorov Smirnoff test was not normal. $P < 0.05$ was considered significant.

Results

TLR2 expression is linked to poor prognosis in BC patients

To investigate whether TLR2 expression correlates with prognosis in BC patients, we performed a meta-analysis on public gene-expression data from human breast tumors [15]. Patients with high TLR2 expression showed lower RFS (Fig. 1A and Supplementary Fig. 1) and OS (Fig. 1B) than those with low TLR2, suggesting that TLR2 may play a role in BC progression.

TLR2 deletion hinders HER2-driven mammary carcinogenesis

To study the role of TLR2 in mammary carcinogenesis and progression, we generated neuT-TLR2^{WT} and neuT-TLR2^{KO} mice, which carry the activated rat HER2/neu oncogene under the MMTV promoter and spontaneously develop mammary tumors. Tumor onset was significantly delayed in neuT-TLR2^{KO} mice (Fig. 1C), which displayed significantly higher survival and a decrease in tumor multiplicity compared to neuT-TLR2^{WT} mice (Fig. 1D-F). This was accompanied by a lower frequency of aldehyde dehydrogenase 1^{+} (Aldefluor^{+}), Sca1^{+} and CD44^{+}CD24^{-} CSCs [28] in neuT-TLR2^{KO} tumors than in neuT-TLR2^{WT} (Fig. 1G-I). Moreover, the cells purified from neuT-TLR2^{KO} tumors generated significantly fewer tumorspheres than those from neuT-TLR2^{WT} (Fig. 1J), confirming that TLR2 promotes CSC survival and self-renewal, and plays a key role in HER2-driven mammary carcinogenesis.

TLR2 deletion alters Treg frequency without affecting other immune-cell populations

Since TLR2 is expressed on many immune cells [6], we assessed the percentage of the main immune cell types in the tumors, blood and spleens from neuT-TLR2^{KO} and neuT-TLR2^{WT} mice at the experimental endpoint. While no significant differences were observed in most of the myeloid and lymphoid populations (Fig. 2A, B, E, F, H, I) or in macrophage polarization (Fig. 2D), significantly lower Treg frequency was found in the tumors, blood, and spleens from neuT-TLR2^{KO} mice (Fig 2C, G, J). The lower Treg frequency observed in neuT-TLR2^{KO} was not caused by their lower tumor burden, as significantly lower levels of circulating Tregs were found in tumor-free TLR2^{KO} than in TLR2^{WT} mice (Fig. 2K). Moreover, Tregs express higher TLR2 levels than effector CD4^{+} T cells (Fig. 2L). Interestingly, when circulating T cells from tumor-bearing TLR2^{WT} mice were activated in the presence of TLR2 activators,

PGN-SA or HMGB1, the percentage of Tregs was significantly increased compared to the control (Fig. 2M), demonstrating that TLR2 directly promotes Treg expansion.

TLR2 promotes BC progression mostly via cancer-cell-intrinsic mechanisms

To assess whether TLR2 signaling provides the major contribution to tumor progression in cancer cells or whether other $TLR2^{+}$ cells are involved, we generated cell lines from the primary tumors of neuT-$TLR2^{WT}$ and neuT-$TLR2^{KO}$ mice, named WT-874, and KO-M26 and KO-E26, respectively. All these cells express HER2 and the luminal marker cytokeratin 19 (CK19) but are negative for the basal marker alpha smooth muscle actin (α-SMA) (Supplementary Figure 2A-C) and proliferate at a similar rate *in-vitro* (not shown).

We performed the orthotopic cross transplantation of WT-874 and KO-M26 cells into $TLR2^{WT}$ and $TLR2^{KO}$ mice. Tumor onset and progression strictly correlated to the presence of TLR2 in cancer cells. Indeed, WT-874 cells generated tumors in 100% of mice, regardless of genetic background of the recipient, while KO-M26 cells generated tumors in only 20% and 30% of $TLR2^{WT}$ and $TLR2^{KO}$ mice, respectively (Fig. 3A). Moreover, the tumors generated by KO-M26 cells remained very small (mean diameters at sacrifice < 2 mm), regardless of the genetic background of the receiving mice (Fig. 3B). The tumors generated by WT-874 cells injected into $TLR2^{KO}$ mice were significantly larger (mean diameters at sacrifice < 5 mm), and significantly bigger tumors were generated by the WT-874 cells injected into $TLR2^{WT}$ mice (mean diameters at sacrifice: 10 mm) (Fig. 3B). Similar results were obtained using KO-E26 cells (Supplementary Figure 3).

To confirm the TLR2 tumor-cell-intrinsic mechanisms, 4T1 cells were silenced for TLR2 and injected into syngeneic BALB/c mice. TLR2 silencing significantly impaired tumor growth compared to control cells (Fig. 3C). Moreover, the transplantation experiment was repeated in NSG mice to understand whether the ability of $TLR2^{+}$ tumors to shape an immunosuppressive TME is the major contribution to tumor progression, or whether their tumorigenic properties are tumor-cell-intrinsic. KO-M26 and KO-E26 cells generated smaller tumors than WT-874 cells, although all the tumors grew faster than in immunocompetent mice (Fig. 3D). These results, and the observations on Tregs, indicate that the TLR2-dependent pro-tumor effect is mostly cancer-cell intrinsic, although host TLR2-expressing cells provide a partial contribution.

TLR2 promotes CSC self-renewal and its inhibition impairs cell viability

We then exploited WT-874, KO-M26 and KO-E26 to characterize the tumor-cell-intrinsic pro-carcinogenic effects of TLR2. As expected, TLR2 was expressed on the cell surface of WT-874 cells, as well as on other murine or human mammary cancer cell lines, while was absent in KO-M26 and KO-E26 cells (Fig. 4A). When cultured in tumorsphere-forming conditions, the WT-874 cells generated significantly more tumorspheres than KO-M26 and KO-E26 (Fig. 4B), in accordance with the higher frequency of $CD44^{+}CD24^{-}$ CSCs (Supplementary Fig. 2 D). Moreover, the percentage of $Aldefluor^{+}$ cells was higher in the CSC-enriched P1 tumorspheres of all three cell lines than in 2D cultures, but was significantly higher

in the WT-874 cells under both conditions (Fig. 4B), confirming that TLR2 induces CSC self-renewal. Moreover, TLR2 induces the secretion of pro-tumoral cytokines, since, compared to KO-M26 or KO-E26 cells, WT-874 produced significantly higher amounts of TGF-β, IL-6 and VEGF (Fig. 4C-E), which are responsible for triggering a pro-tumoral loop that promotes CSC self-renewal, proliferation and invasion [8].

Several mouse and human BC cell lines, including TUBO, 4T1 and MDA-MB-231, express TLR2 (Fig. 4A). We therefore assessed the effect of TLR2 activation on their tumorsphere-generation ability. Murine $HER2^+$ TUBO and TNBC 4T1 cells were stimulated with PGN-SA or HMGB1. Under these stimuli, TUBO and 4T1 cells generated significantly more spheres and expressed higher levels of the CSC marker Sca1 than control cells (Fig. 4F, G and Supplementary Fig. 4). This effect was TLR2-dependent, as was not observed in TLR2-silenced cells (Fig. 4F, G). PGN-SA and HMGB1 also increased tumorsphere generation in human TNBC MDA-MB-231 cells (Fig. 4H).

We therefore hypothesize that TLR2 inhibition impairs BC cell viability. Indeed, the TLR2 inhibitor CU-CPT-22 dose-dependently impaired WT-874, TUBO, 4T1 and MDA-MB-231 cell viability (Fig. 4I), while it was ineffective on KO-M26 or KO-E26 cells (not shown). Overall, these results demonstrate that TLR2 signaling promotes breast CSC self-renewal, and that its inhibition affects BC cell viability.

TLR2 mediates resistance to chemotherapy

High TLR2 expression in BC patients correlates with a significantly impaired response to chemotherapy, as chemotherapy-treated BC patients with $TLR2^{high}$ tumors showed lower RFS than patients with $TLR2^{low}$ tumors (Fig. 5A), and TLR2 expression was significantly higher in non-responder than responder patients (Fig. 5B). Accordingly, WT-874 cells were more resistant to doxorubicin than KO-M26 and KO-E26 cells, which showed lower viability (Fig. 5C) and significantly higher apoptosis (Fig. 5D) in response to doxorubicin. Interestingly, TLR2 inhibition with CU-CPT-22 increased the sensitivity of $HER2^+$ (WT-874 and TUBO) and TN (4T1 and MDA-MB-231) BC cells to doxorubicin (Fig. 5E). Significantly, the two drugs in combination exerted synergistic activity, as calculated using the Bliss independence model (Fig. 5F). We analyzed the supernatants of doxorubicin-treated cells to dissect the mechanisms involved in TLR2-dependent chemoresistance, and found that doxorubicin induced the release of HMGB1, which may activate TLR2, in all BC cells tested, with higher amounts released by KO-M26 and KO-E26 cells, which is in line with their higher sensitivity to doxorubicin (Fig. 5G). Treatment with HMGB1 induced the phosphorylation of the TLR2 downstream signal transducer p65 NF-κB in WT-874 cells, but not in KO-M26 and KO-E26 cells (Fig. 5H). As expected, doxorubicin induced NF-κB phosphorylation in WT-874, TUBO, 4T1 and MDA-MB-231 cells, while TLR2 inhibition with CU-CPT-22 significantly reduced NF-κB activation. The addition of CU-CPT-22 to doxorubicin-treated cells significantly reduced NF-κB phosphorylation in all cell lines (Fig. 5I). Moreover, doxorubicin treatment induced the release, from WT-874, TUBO and 4T1 cells, of NF-κB-regulated cytokine IL-6, which was abolished by adding CU-CPT-22 (Supplementary Fig. 5). Since NF-κB inhibits apoptosis and promotes cell survival [6], CU-CPT-22 synergized with doxorubicin and significantly improved its apoptotic effect in WT-874, TUBO, 4T1 and

MDA-MB-231 cells (Fig. 5J). This effect was not due to off-target mechanisms, as CU-CPT-22 treatment did not exert any effect on KO-M26 or KO-E26 cells (Supplementary Fig. 6A-B). Interestingly, CU-CPT-22 increased doxorubicin-induced apoptosis to a similar extent as treatment with NF-κB inhibitor BAY 11-7082 (Supplementary Fig. 6C) and HMGB1 antagonist BOX-A (Supplementary Fig. 6D).

These results demonstrate that TLR2/NF-κB signaling, which is activated by doxorubicin-induced HMGB1 release, plays an essential role in chemoresistance, and that TLR2 inhibition restores BC cell sensitivity to chemotherapy.

Treatment with a TLR2 inhibitor potentiates doxorubicin anti-cancer effects *in-vivo*

To verify whether TLR2 inhibition exerts an antitumor effect *in-vivo*, we prepared a therapeutic model to treat 4T1 tumor-bearing BALB/c mice with two different doses of CU-CPT-22 (10 or 50 μg) intratumorally, twice per week, starting when tumors reached 2 mm in mean diameter. Both CU-CPT-22 doses significantly reduced tumor growth, and treatment at 50 μg significantly reduced the number of spontaneous lung metastases (Supplementary Fig. 7). We then analyzed whether CU-CPT-22 synergizes with chemotherapy to hinder BC growth; 4T1 tumor-bearing mice were treated with doxorubicin, with and without CU-CPT-22 (50 μg), twice per week. Both doxorubicin and CU-CPT-22, administered as single treatments, significantly reduced tumor growth compared to control mice (Fig. 6A). The combination of doxorubicin and CU-CPT-22 induced a statistically significant reduction in tumor growth compared to the two single treatments (Fig. 6A). Moreover, mice treated with CU-CPT-22 + doxorubicin showed significantly fewer lung metastases than control- or doxorubicin-group mice (Fig. 6B). A cytofluorimetric analysis of tumors showed that the combination of CU-CPT-22 and doxorubicin induced a statistically significant decrease in $Sca1^+$ CSCs compared to tumors from mice treated with doxorubicin alone, demonstrating that CU-CPT-22 synergizes with doxorubicin impairing CSC survival *in-vivo* (Fig. 6C). Moreover, the combined therapy induced a significant increase in tumor-infiltrating $CD8^+$ T cells and a decrease in Tregs (Fig. 6D, E), while no significant differences in $CD4^+$ T, NK cells or M0, M1 and M2 macrophages were observed (not shown). Mice underwent MRI at the experimental end point to better characterize the effects of the combination treatment. T_{2w} morphological axial and coronal MR images were acquired at B_0 = 7T. As shown in the representative T_{2w} axial images, a significant decrease in tumor volume occurred upon treatment with CU-CPT-22 + doxorubicin (Fig. 6F, *up*). The MRI quantification of tumor volume showed decreases of 38±2%, 47±10% and 75±16% in mice treated with CU-CPT-22, doxorubicin, or both, respectively, compared to control mice (Fig. 6G). ADC-MRI maps, which report the degree of freedom of water, were obtained using DWI-MRI. False color representative axial ADC maps of the tumor region (superimposed onto morphological T_{2w} MR images) are reported in Fig. 6F (*lower*) for control mice and mice treated with doxorubicin and CU-CPT-22 simultaneously. A significant higher ADC value, an indication of decreased cellularity, was observed in CU-CPT-22 + doxorubicin-treated mice than in control mice, while no significant effect was detected in mice treated with doxorubicin or CU-CPT-22 alone (Fig. 6H). Overall, these data indicate that treatment with TLR2 inhibitors synergizes with

chemotherapy, reducing breast tumor growth and metastatic dissemination, and restoring an immunocompetent TME.

Discussion

Chemotherapy is still the main option for TNBC and metastatic BC patients, with neoadjuvant and adjuvant chemotherapy becoming mainstays for treating early BC. However, chemoresistance is common in both advanced and early BC, and about 30% of early-stage BC patients relapse despite treatment [3, 29]. Therefore, the development of combined treatments to counteract chemoresistance and strengthen anti-cancer activity is an urgent medical need.

Since breast CSCs are chemotherapy resistant and involved in tumor relapse [30], we have previously sought genes that play a key role in breast CSC survival. We identified TLR2 as being overexpressed in breast CSCs and as playing a role in their self-renewal [8]. Herein, we have analyzed TLR2's role in mammary carcinogenesis by generating genetically modified mice that, to our knowledge, represent the only model of HER2-driven mammary carcinogenesis on a $TLR2^{KO}$ background. We thus demonstrated for the first time that TLR2 knockout impairs HER2-driven spontaneous mammary carcinogenesis, delaying tumor onset and decreasing tumor multiplicity. These results mirror observations in BC patients, whose tumors express higher TLR2 levels than adjacent normal tissue and in which high tumor TLR2 expression is associated with poor prognosis [31]. Significantly, several genetic alterations that result in increased TLR2-signaling-pathway activation, including mutations that generate constitutively active forms of TLR2 and amplifications in TLR2 downstream effector *IRAK1* (observed in 23.8% of patients), have been identified in BC patients [32].

The pro-tumorigenic role of TLR2 is, at least partly, mediated by its ability to promote breast-CSC self-renewal, as demonstrated by the higher frequency of cells that express typical breast CSC markers, and the enhanced ability of BC from TLR2-expressing mice to generate CSC-enriched tumorspheres compared to their $TLR2^{KO}$ counterparts. Indeed, we have previously demonstrated that TLR2 stimulation in breast CSCs leads to the activation of the MyD88/NF-κB and AKT pathways, which promote the secretion of several cytokines and growth factors, such as TGF-β, IL-6 and VEGF [8]. These factors promote CSC survival, self-renewal and invasion via the activation of the STAT3 and Smad3 pathways [6, 33], in accordance with data that show increased TLR2 expression in BC cell lines endowed with metastatic potential [34]. The central role played by tumor-cell-intrinsic TLR2-dependent mechanisms in mediating pro-tumorigenic effects is confirmed by our transplantation experiments; unlike $TLR2^{WT}$ BC cells, $TLR2^{KO}$ BC cells have a poor ability to generate tumors when injected into both immunocompetent and NSG mice. However, host-cell TLR2 also contributes to tumor progression, as $TLR2^{KO}$ mice represented a more hostile environment than $TLR2^{WT}$ mice for the growth of $TLR2^{+}$ BC. This suggests that TLR2 expression on immune cells may contribute to their immunosuppressive activity. In fact, several research groups have demonstrated that TLR2 stimulation in myeloid-derived suppressor cells induces their accumulation in the TME and lymphoid organs [35], and the production of IL-6 and IL-10, which polarize M2

macrophages and favor metastatic dissemination [36, 37]. Moreover, TLR2 has been shown to promote Treg proliferation both directly, through the TLR2–MyD88–NF-κB axis [38], and indirectly, via the activation of dysfunctional dendritic cells that produce IL-6 and IL-10 [39]. Fittingly, we observed a decrease in both tumor-infiltrating and peripheral Tregs in tumor-bearing neuT-TLR2^{KO}, compared to neuT-TLR2^{WT} mice. This decrease was not due to the lower tumor burden in neuT-TLR2^{KO} mice, since healthy, non neuT, TLR2^{KO} mice showed a lower percentage of circulating Tregs than TLR2^{WT} mice. We confirmed *in-vitro* that TLR2 activation in T cells directly promotes the expansion of Tregs, which express higher TLR2 levels than effector CD4^{+} T cells, demonstrating that TLR2 plays an important role in Treg biology. However, TLR2 deficiency did not affect the percentages of other immune populations, whether in the tumor or periphery. Nevertheless, further studies are required to demonstrate their functional integrity.

Besides its direct role in breast carcinogenesis, TLR2 plays a role in BC chemoresistance, as high TLR2 expression correlates with low RFS in chemotherapy-treated BC patients. Furthermore, the deletion or pharmacologic inhibition of TLR2 increases the sensitivity of several BC cell lines to doxorubicin. This mechanism of chemoresistance is mediated by the release of TLR2-activating DAMPs, such as HMGB1, following doxorubicin-induced immunogenic cell death. The binding of HMGB1 to TLR2 activates the NF-κB signaling pathway, inducing the production of IL-6, a well-known promoter of survival, growth and proliferation in both immunosuppressive and cancer cells [40, 41], thus protecting cells from apoptosis. Indeed, high HMGB1 levels correlate with poor response to neoadjuvant chemotherapy in TNBC patients [10], and HMGB1 protects BC cells from chemotherapy and promotes metastasis formation [42]. Moreover, other DAMPs that can activate TLR2 may be released into the TME following chemotherapy [6, 43]. Interestingly, bacteria may induce TLR2 activation. A specific microbiota has recently been found in mammary glands, with normal and neoplastic samples showing alterations in amount and composition [44]. Neoadjuvant chemotherapy changes breast microbiota composition, inducing an increase in *Pseudomonas aeruginosa*, a potential TLR2 activator that stimulates BC cell proliferation [45]. Moreover, many chemotherapy-treated patients suffer from opportunistic infections from Gram-positive bacteria, with the commensal bacteria diffusing to the tumor, which could further activate TLR2 [46]. Therefore, the administration of TLR2 inhibitors in combination with chemotherapy might not only impair the pro-inflammatory and pro-tumorigenic activity of HMGB1 and other DAMPs but may also counteract some of the detrimental effects of breast dysbiosis. Further experiments are needed to confirm this hypothesis.

Our *in-vivo* therapeutic experiments have demonstrated that treatment with TLR2 inhibitor CU-CPT-22 synergized with doxorubicin in hampering BC progression, potentiating its anti-cancer effects and decreasing metastatic dissemination. The combination of doxorubicin and TLR2 inhibition significantly decreased CSC frequency and altered the immune-infiltrate composition, inducing an increase in CD8^{+} T cells and a decrease in Tregs, thus generating a more anti-tumor TME. The synergistic effect of this combined treatment was confirmed by MRI, which identified a significant reduction in tumor volume (about 75%), compared to control mice, and more heterogeneous tumor morphology, with a significant reduction in necrotic area. Further insights into tumor features have been gained by using DWI-MRI to obtain ADC maps that report the degree of freedom of water, which is a technique that is extensively

applied to assess increases in cellularity during tumor growth [27]. Treatment with doxorubicin and CU-CPT-22 caused an increase in water freedom, suggesting a lowering of cellularity because of tumor regression.

Significantly, although TLR2 is expressed on immune cells, no detrimental alterations in the immune system were observed in mice treated with CU-CPT-22 and $TLR2^{KO}$ mice, which supports the safety and feasibility of TLR2 targeting. Indeed, innate and acquired immune responses are well-preserved in the absence of TLR2 [47]. TLR2 inhibitors (monoclonal antibodies or small molecule inhibitors) have so far been successfully used in clinical trials for the treatment of acute myeloid leukemia and myelodysplastic syndrome [48, 49]. Our data suggest that this approach may also benefit patients suffering from solid tumors.

Conclusions

Herein, we have identified a new mechanism of BC chemoresistance activated by chemotherapy-induced release of HMGB1, which stimulates TLR2 pro-survival effects. We have thus demonstrated that TLR2 targeting restores sensitivity to chemotherapy. The combined use of standard therapies and TLR2 inhibition is therefore an attractive strategy for BC treatment (Fig. 6J).

Abbreviations

α-SMA: alpha smooth muscle actin

ADC: Apparent diffusion constant

BC: breast cancer

CK19: cytokeratin 19

CSC: cancer stem cells

DAMP: damage-associated molecular patterns

DWI-MRI: Diffusion Weighted Magnetic Resonance Imaging

ER: estrogen receptor

G-CSF: granulocytic-colony stimulating factor

HMGB1: high mobility group box 1

IL: interleukin

i.p.: intraperitoneal

MRI: Magnetic Resonance Imaging

NSG: NOD SCID gamma

OS: overall survival

PGN-SA: peptidoglycan from S. aureus

PRR: pattern recognition receptors

RARE: Rapid Acquisition with Refocused Echoes

RFS: relapse-free survival

TGF-b: tumor growth factor

TLR2: Toll-like Receptor 2

TME: Tumor microenvironment

TNBC: triple negative breast cancer

Treg: T regulatory cell

VEGF: vascular endothelial growth factor

Declarations

Ethics approval and consent to participate: Mice were bred and maintained under saprophytic and pathogen-free conditions at the animal facility of the Molecular Biotechnology Center, and treated in accordance with EU and institutional guidelines, with the approval of the Animal Care and Use Committee of University of Turin and of the Italian Ministry of Health (authorizations N° 107/2020-PR and 500/2017-PR).

Consent for publication: Not applicable

Availability of data and materials: All data generated or analyzed during this study are included in this published article and its supplementary information files.

Competing interests: The authors declare that they have no competing interests.

Funding: The research leading to these results has received funding from AIRC under the IG 2015 – ID. 16724 and IG 2018 - ID. 21468 projects – principal investigator F. Cavallo, from Fondazione Ricerca Molinette Onlus, and from the University of Turin (Turin, Italy). The Italian Ministry for University and Research (MUR) is gratefully acknowledged for yearly FOE funding to the Euro-BioImaging Multi-Modal Molecular Imaging Italian Node (MMMI).

Authors' contributions: L.C. and F.C. designed the project and the experiments. L.C., A.D.L. and E.B. wrote the paper, and F.C. and E.Q. reviewed it. E.B., A.D.L., I.F.M., F.R., L.A. and R.R. performed experiments and analyzed the data. G.F. and E.D.G. performed and analyzed MRI. L.C. and F.C. coordinated and directed the study. All authors have read and approved the final version of the manuscript.

Acknowledgements: We thank Dr. Dale Lawson for his revision and editing of the manuscript.

References

1. Sung H, Ferlay J, Siegel RL, Laversanne M, Soerjomataram I, Jemal A, Bray F: **Global cancer statistics 2020: GLOBOCAN estimates of incidence and mortality worldwide for 36 cancers in 185 countries**. *CA Cancer J Clin* 2021.
2. Ayala de la Pena F, Andres R, Garcia-Saenz JA, Manso L, Margeli M, Dalmau E, Pernas S, Prat A, Servitja S, Ciruelos E: **SEOM clinical guidelines in early stage breast cancer (2018)**. *Clin Transl Oncol* 2019, **21**:18–30.
3. Nigdelis MP, Karamouzis MV, Kontos M, Alexandrou A, Goulis DG, Lambrinoudaki I: **Updates on the treatment of invasive breast cancer**: **Quo Vadimus?** *Maturitas* 2021, **145**:64-72.
4. Ji X, Lu Y, Tian H, Meng X, Wei M, Cho WC: **Chemoresistance mechanisms of breast cancer and their countermeasures**. *Biomed Pharmacother* 2019, **114**:108800.
5. Conti L, Ruiu R, Barutello G, Macagno M, Bandini S, Cavallo F, Lanzardo S: **Microenvironment, oncoantigens, and antitumor vaccination: lessons learned from BALB-neuT mice**. *Biomed Res Int* 2014, **2014**:534969.
6. Di Lorenzo A, Bolli E, Tarone L, Cavallo F, Conti L: **Toll-Like Receptor 2 at the Crossroad between Cancer Cells, the Immune System, and the Microbiota**. *Int J Mol Sci* 2020, **21**.
7. Pandey S, Singh S, Anang V, Bhatt AN, Natarajan K, Dwarakanath BS: **Pattern Recognition Receptors in Cancer Progression and Metastasis**. *Cancer Growth Metastasis* 2015, **8**:25–34.
8. Conti L, Lanzardo S, Arigoni M, Antonazzo R, Radaelli E, Cantarella D, Calogero RA, Cavallo F: **The noninflammatory role of high mobility group box 1/Toll-like receptor 2 axis in the self-renewal of mammary cancer stem cells**. *FASEB J* 2013, **27**:4731–4744.
9. Bianchi ME, Crippa MP, Manfredi AA, Mezzapelle R, Rovere Querini P, Venereau E: **High-mobility group box 1 protein orchestrates responses to tissue damage via inflammation, innate and adaptive immunity, and tissue repair**. *Immunol Rev* 2017, **280**:74–82.
10. Tanabe Y, Tsuda H, Yoshida M, Yunokawa M, Yonemori K, Shimizu C, Yamamoto S, Kinoshita T, Fujiwara Y, Tamura K: **Pathological features of triple-negative breast cancers that showed progressive disease during neoadjuvant chemotherapy**. *Cancer Sci* 2017, **108**:1520–1529.
11. Rovero S, Amici A, Di Carlo E, Bei R, Nanni P, Quaglino E, Porcedda P, Boggio K, Smorlesi A, Lollini PL, et al: **DNA vaccination against rat her-2/Neu p185 more effectively inhibits carcinogenesis than transplantable carcinomas in transgenic BALB/c mice**. *J Immunol* 2000, **165**:5133–5142.

12. Liu S, Chen H: **Isolation of Primary Breast Cancer Cells from HER2 Transgenic Mice**. *Bio-protocol* 2016, **6**:e1956.
13. Geninatti Crich S, Cadenazzi M, Lanzardo S, Conti L, Ruiu R, Alberti D, Cavallo F, Cutrin JC, Aime S: **Targeting ferritin receptors for the selective delivery of imaging and therapeutic agents to breast cancer cells**. *Nanoscale* 2015, **7**:6527–6533.
14. Pawitan Y, Bjohle J, Amler L, Borg AL, Egyhazi S, Hall P, Han X, Holmberg L, Huang F, Klaar S, et al: **Gene expression profiling spares early breast cancer patients from adjuvant therapy: derived and validated in two population-based cohorts**. *Breast Cancer Res* 2005, **7**:R953-964.
15. 2021 K-MphkcaAotM.
16. Győrffy B, Lanczky A, Eklund AC, Denkert C, Budczies J, Li Q, Szallasi Z: **An online survival analysis tool to rapidly assess the effect of 22,277 genes on breast cancer prognosis using microarray data of 1,809 patients**. *Breast Cancer Research and Treatment* 2010, **123**:725–731.
17. Fekete JT, Gyorffy B: **ROCplot.org: Validating predictive biomarkers of chemotherapy/hormonal therapy/anti-HER2 therapy using transcriptomic data of 3,104 breast cancer patients**. *Int J Cancer* 2019, **145**:3140–3151.
18. 2021. RPhwroAotA.
19. Lanzardo S, Conti L, Rooke R, Ruiu R, Accart N, Bolli E, Arigoni M, Macagno M, Barrera G, Pizzimenti S, et al: **Immunotargeting of Antigen xCT Attenuates Stem-like Cell Behavior and Metastatic Progression in Breast Cancer**. *Cancer Res* 2016, **76**:62–72.
20. Conti L, De Palma R, Rolla S, Boselli D, Rodolico G, Kaur S, Silvennoinen O, Niccolai E, Amedei A, Ivaldi F, et al: **Th17 cells in multiple sclerosis express higher levels of JAK2, which increases their surface expression of IFN-gammaR2**. *J Immunol* 2012, **188**:1011–1018.
21. Conti L, Bolli E, Di Lorenzo A, Franceschi V, Macchi F, Riccardo F, Ruiu R, Russo L, Quaglino E, Donofrio G, Cavallo F: **Immunotargeting of the xCT cystine/glutamate antiporter potentiates the efficacy of Her2-targeted immunotherapies in breast cancer**. *Cancer Immunol Res* 2020.
22. Bandini S, Macagno M, Hysi A, Lanzardo S, Conti L, Bello A, Riccardo F, Ruiu R, Merighi IF, Forni G, et al: **The non-inflammatory role of C1q during Her2/neu-driven mammary carcinogenesis**. *Oncoimmunology* 2016, **5**:e1253653.
23. Donofrio G, Tebaldi G, Lanzardo S, Ruiu R, Bolli E, Ballatore A, Rolih V, Macchi F, Conti L, Cavallo F: **Bovine herpesvirus 4-based vector delivering the full length xCT DNA efficiently protects mice from mammary cancer metastases by targeting cancer stem cells**. *Oncoimmunology* 2018, **7**:e1494108.
24. Macagno M, Bandini S, Stramucci L, Quaglino E, Conti L, Balmas E, Smyth MJ, Lollini PL, Musiani P, Forni G, et al: **Multiple roles of perforin in hampering ERBB-2 (Her-2/neu) carcinogenesis in transgenic male mice**. *J Immunol* 2014, **192**:5434–5441.
25. Conti L, Lanzardo S, Ruiu R, Cadenazzi M, Cavallo F, Aime S, Crich SG: **L-Ferritin targets breast cancer stem cells and delivers therapeutic and imaging agents**. *Oncotarget* 2016.
26. She S, Zhao Y, Kang B, Chen C, Chen X, Zhang X, Chen W, Dan S, Wang H, Wang YJ, Zhao J: **Combined inhibition of JAK1/2 and DNMT1 by newly identified small-molecule compounds**

synergistically suppresses the survival and proliferation of cervical cancer cells. *Cell Death Dis* 2020, **11**:724.

27. Ferrauto G, Di Gregorio E, Lanzardo S, Ciolli L, Iezzi M, Aime S: **Generation of multiparametric MRI maps by using Gd-labelled- RBCs reveals phenotypes and stages of murine prostate cancer**. *Sci Rep* 2018, **8**:10567.
28. Tallerico R, Conti L, Lanzardo S, Sottile R, Garofalo C, Wagner AK, Johansson MH, Cristiani CM, Karre K, Carbone E, Cavallo F: **NK cells control breast cancer and related cancer stem cell hematological spread**. *Oncoimmunology* 2017, **6**:e1284718.
29. Fisusi FA, Akala EO: **Drug Combinations in Breast Cancer Therapy**. *Pharm Nanotechnol* 2019, **7**:3–23.
30. Quaglino E, Conti L, Cavallo F: **Breast cancer stem cell antigens as targets for immunotherapy**. *Semin Immunol* 2020:101386.
31. Wang Y, Liu S, Zhang Y, Yang J: **Dysregulation of TLR2 Serves as a Prognostic Biomarker in Breast Cancer and Predicts Resistance to Endocrine Therapy in the Luminal B Subtype**. *Front Oncol* 2020, **10**:547.
32. Scheeren FA, Kuo AH, van Weele LJ, Cai S, Glykofridis I, Sikandar SS, Zabala M, Qian D, Lam JS, Johnston D, et al: **A cell-intrinsic role for TLR2-MYD88 in intestinal and breast epithelia and oncogenesis**. *Nat Cell Biol* 2014, **16**:1238–1248.
33. Quaglino E, Cavallo F, Conti L: **Cancer stem cell antigens as targets for new combined anti-cancer therapies**. *Int J Biochem Cell Biol* 2020:105861.
34. Xie W, Huang Y, Xie W, Guo A, Wu W: **Bacteria peptidoglycan promoted breast cancer cell invasiveness and adhesiveness by targeting toll-like receptor 2 in the cancer cells**. *PLoS One* 2010, **5**:e10850.
35. Maruyama A, Shime H, Takeda Y, Azuma M, Matsumoto M, Seya T: **Pam2 lipopeptides systemically increase myeloid-derived suppressor cells through TLR2 signaling**. *Biochem Biophys Res Commun* 2015, **457**:445–450.
36. Kim S, Takahashi H, Lin WW, Descargues P, Grivennikov S, Kim Y, Luo JL, Karin M: **Carcinoma-produced factors activate myeloid cells through TLR2 to stimulate metastasis**. *Nature* 2009, **457**:102–106.
37. Sinha P, Clements VK, Bunt SK, Albelda SM, Ostrand-Rosenberg S: **Cross-talk between myeloid-derived suppressor cells and macrophages subverts tumor immunity toward a type 2 response**. *J Immunol* 2007, **179**:977–983.
38. Chen YQ, Li PC, Pan N, Gao R, Wen ZF, Zhang TY, Huang F, Wu FY, Ou XL, Zhang JP, et al: **Tumor-released autophagosomes induces CD4(+) T cell-mediated immunosuppression via a TLR2-IL-6 cascade**. *J Immunother Cancer* 2019, **7**:178.
39. Tang M, Diao J, Gu H, Khatri I, Zhao J, Cattral MS: **Toll-like Receptor 2 Activation Promotes Tumor Dendritic Cell Dysfunction by Regulating IL-6 and IL-10 Receptor Signaling**. *Cell Rep* 2015, **13**:2851–2864.

40. Regis G, Icardi L, Conti L, Chiarle R, Piva R, Giovarelli M, Poli V, Novelli F: **IL-6, but not IFN-gamma, triggers apoptosis and inhibits in vivo growth of human malignant T cells on STAT3 silencing**. *Leukemia* 2009, **23**:2102–2108.
41. Masjedi A, Hashemi V, Hojjat-Farsangi M, Ghalamfarsa G, Azizi G, Yousefi M, Jadidi-Niaragh F: **The significant role of interleukin-6 and its signaling pathway in the immunopathogenesis and treatment of breast cancer**. *Biomed Pharmacother* 2018, **108**:1415–1424.
42. Sohun M, Shen H: **The implication and potential applications of high-mobility group box 1 protein in breast cancer**. *Ann Transl Med* 2016, **4**:217.
43. Secli L, Avalle L, Poggio P, Fragale G, Cannata C, Conti L, Iannucci A, Carra G, Rubinetto C, Miniscalco B, et al: **Targeting the extracellular HSP90 co-chaperone Morgana inhibits cancer cell migration and promotes anti-cancer immunity**. *Cancer Res* 2021.
44. Fernandez MF, Reina-Perez I, Astorga JM, Rodriguez-Carrillo A, Plaza-Diaz J, Fontana L: **Breast Cancer and Its Relationship with the Microbiota**. *Int J Environ Res Public Health* 2018, **15**.
45. Chiba A, Bawaneh A, Velazquez C, Clear KYJ, Wilson AS, Howard-McNatt M, Levine EA, Levi-Polyachenko N, Yates-Alston SA, Diggle SP, et al: **Neoadjuvant Chemotherapy Shifts Breast Tumor Microbiota Populations to Regulate Drug Responsiveness and the Development of Metastasis**. *Mol Cancer Res* 2020, **18**:130–139.
46. Montassier E, Gastinne T, Vangay P, Al-Ghalith GA, Bruley des Varannes S, Massart S, Moreau P, Potel G, de La Cochetiere MF, Batard E, Knights D: **Chemotherapy-driven dysbiosis in the intestinal microbiome**. *Aliment Pharmacol Ther* 2015, **42**:515–528.
47. Wooten RM, Ma Y, Yoder RA, Brown JP, Weis JH, Zachary JF, Kirschning CJ, Weis JJ: **Toll-like receptor 2 is required for innate, but not acquired, host defense to Borrelia burgdorferi**. *J Immunol* 2002, **168**:348–355.
48. Garcia-Manero G, Montalban-Bravo G, Yang H, Wei Y, Alvarado Y, DiNardo CD, Daver NG, Konopleva M, Hearn KP, Miller R, et al: **A Clinical Study of OPN-305, a Toll-like Receptor 2 (TLR-2) Antibody, in Patients with Lower Risk Myelodysplastic Syndromes (MDS) That Have Received Prior Hypomethylating Agent (HMA) Therapy** *Blood* 2016, **128**.
49. Kovacsovics TJ, Mims A, Salama ME, Pantin J, Rao N, Kosak KM, Ahorukomeye P, Glenn MJ, Deininger MWN, Boucher KM, et al: **Combination of the low anticoagulant heparin CX-01 with chemotherapy for the treatment of acute myeloid leukemia**. *Blood Adv* 2018, **2**:381–389.

Figures

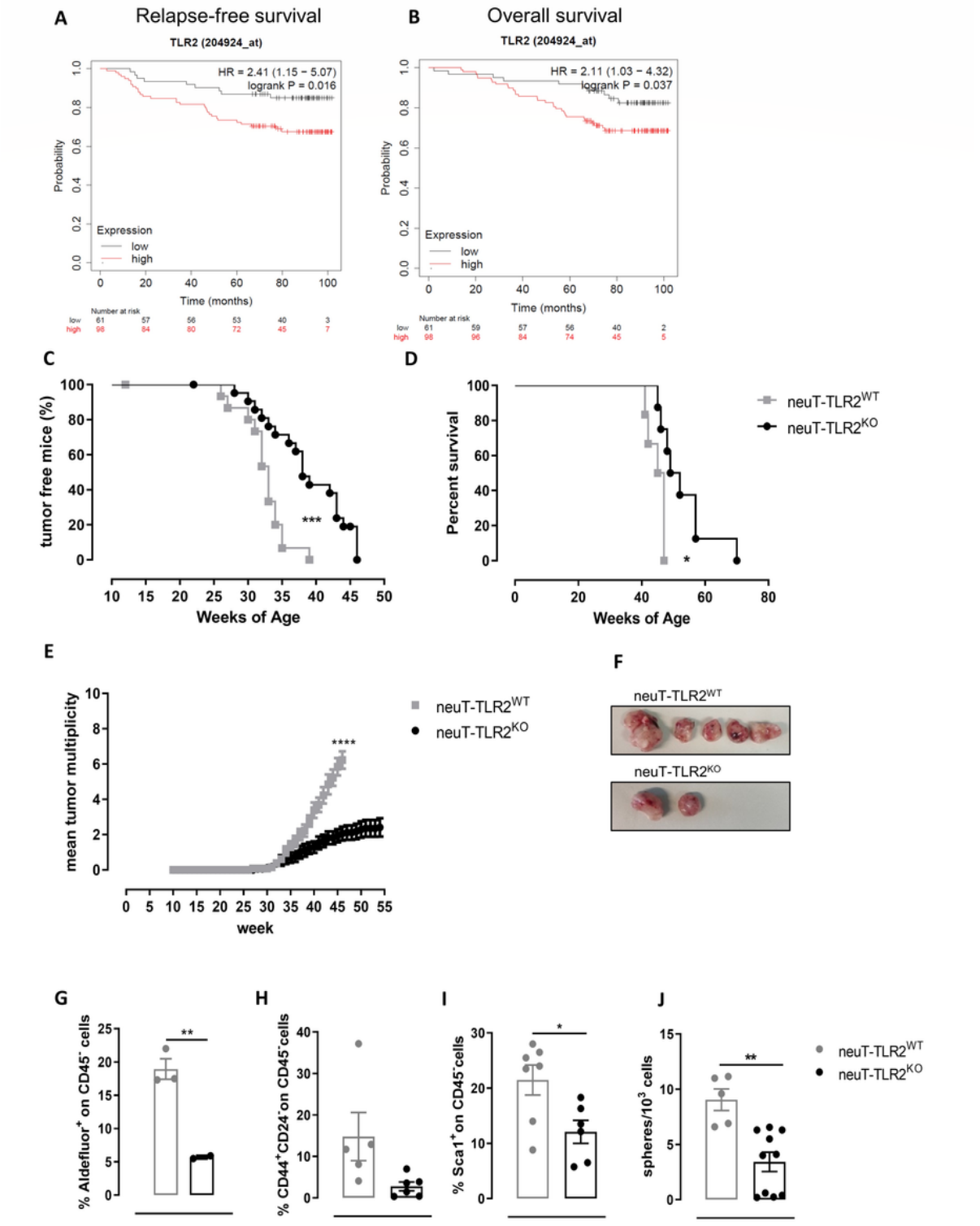

Figure 1

TLR2 correlates with poor prognosis in BC patients, and its deletion hinders HER2-driven mammary carcinogenesis and affects CSCs. (A, B) Kaplan–Meier plots displaying (A) RFS and (B) OS in BC patients from the GSE1456 dataset, stratified according to TLR2 mRNA expression (N = 159). (C) Tumor-free survival, (D) OS, (E) tumor multiplicity and (F) representative images of mammary tumors of neuT-TLR2WT (N = 16) and neuT-TLR2KO (N = 22) mice. (G-I) FACS analysis of (G) Aldefluor+, (H) CD44+CD24-

and (I) Sca1+ CSCs in tumors explanted from neuT-TLR2WT or neuT-TLR2KO mice. Graphs show mean ± SEM of the percentage of CSCs from among CD45- cells (each dot represents a mouse). N ≥ 3 per group. (L) Sphere-generating ability (number of tumorspheres generated every 103 plated cells) of cells dissociated from the tumors of neuT-TLR2WT (N = 5) and neuT-TLR2KO (N = 10) mice.*, P < 0.05; **, P < 0.01; *** P < 0.001; ****, P < 0.0001. (C-D) Log-rank Mantel-Cox and (E, G-L) Student's t tests.

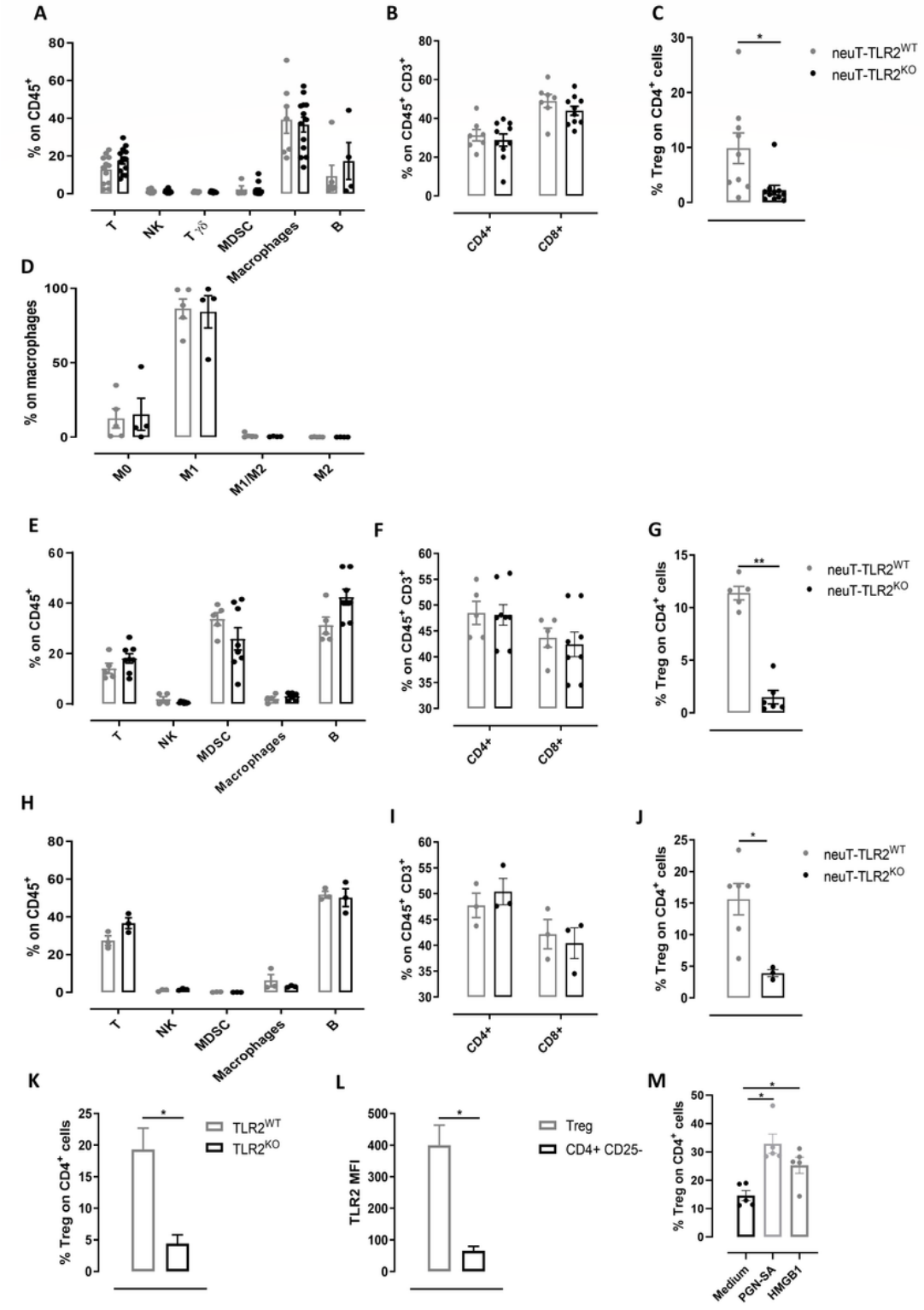

Figure 2

TLR2 deletion alters Treg cell frequency without affecting other immune populations. FACS analysis of immune cells in (A-D) tumors, (E-G) blood and (H-J) spleens from neuT-TLR2KO and neuT-TLR2WT mice. Graphs show mean ± SEM of the percentage of (A, E, H) lymphocytes and myeloid cells from among CD45+ cells, (B, F, I) CD4+ and CD8+ from among CD3+ T cells, (C, G, J) Tregs from among CD4+ T cells and (D) M0, M1, M1/M2 and M2 from among total macrophages. Each dot represents a mouse (N ≥ 3 per group). (K) FACS analysis of peripheral Tregs in TLR2KO and TLR2WT mice. Graphs show mean ± SEM of the percentage of Tregs from among CD4+ T cells. (L) FACS analysis of TLR2 expression on Tregs and CD4+CD25- cells from TLR2WT mice. Graphs show mean ± SEM of TLR2 MFI. (M) FACS analysis of Tregs from TLR2WT mice upon ex-vivo stimulation of blood T lymphocytes with TLR2 activatory ligands. Graphs show mean ± SEM of the percentage of Tregs from among CD4+ cells. Each dot represents a mouse (N = 3 per group). *, P < 0.05; **, P < 0.01; Student's t test.

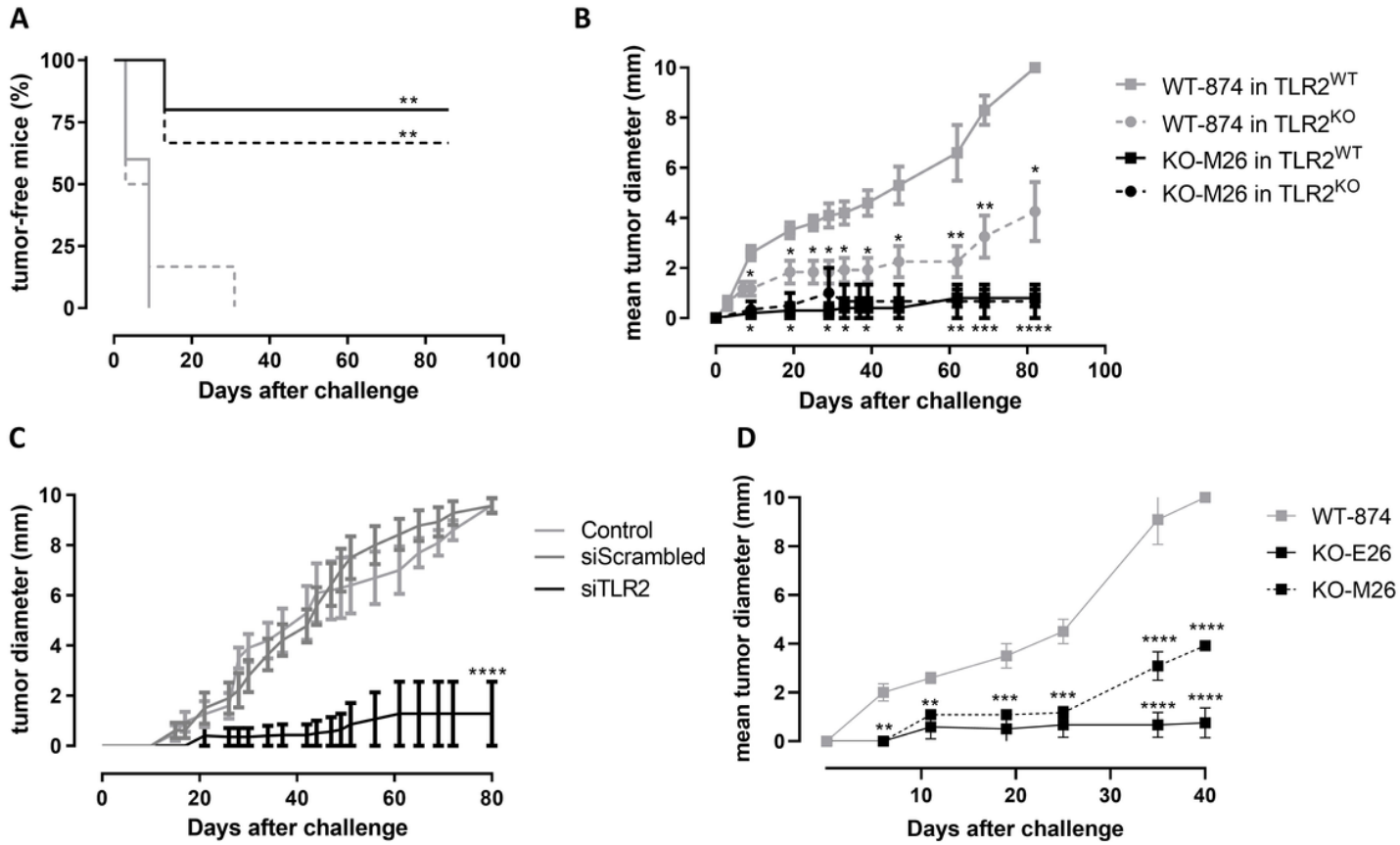

Figure 3

TLR2 promotes BC growth mainly via tumor-cell-intrinsic mechanisms. (A) Tumor-free survival and (B) mean tumor diameter of TLR2WT and TLR2KO mice (N = 6 per group, from 2 independent experiments) injected orthotopically with 1x106 WT-874 or KO-M26 cells. (C) Mean tumor diameter of BALB/c mice orthotopically injected with 1x104 4T1 cells left untreated (N = 5), transfected with scrambled siRNAs (N = 7) or siRNAs to TLR2 (N = 7). ****, P < 0.0001, Kruskal-Wallis test. (D) Mean tumor diameter of NSG mice injected orthotopically with 1x106 WT-874, KO-M26 or KO-E26 cells (N = 6 per group). (A) **, P <

0.01, Log-rank (Mantel-Cox) of KO-M26 cells injected into TLR2WT and TLR2KO mice vs WT-874 cells injected into TLR2WT mice. (B) *, P < 0.05; **, P < 0.01; ***, P < 0.001, Mann Whitney test of KO-M26 cells injected into TLR2WT and TLR2KO mice vs WT-874 cells, and of WT-874 injected into TLR2WT vs TLR2KO mice. (D) **, P < 0.01; ***, P < 0.001; ****, P < 0.0001. Mann Whitney test of WT-874 cells vs KO-M26 and KO-E26 cells.

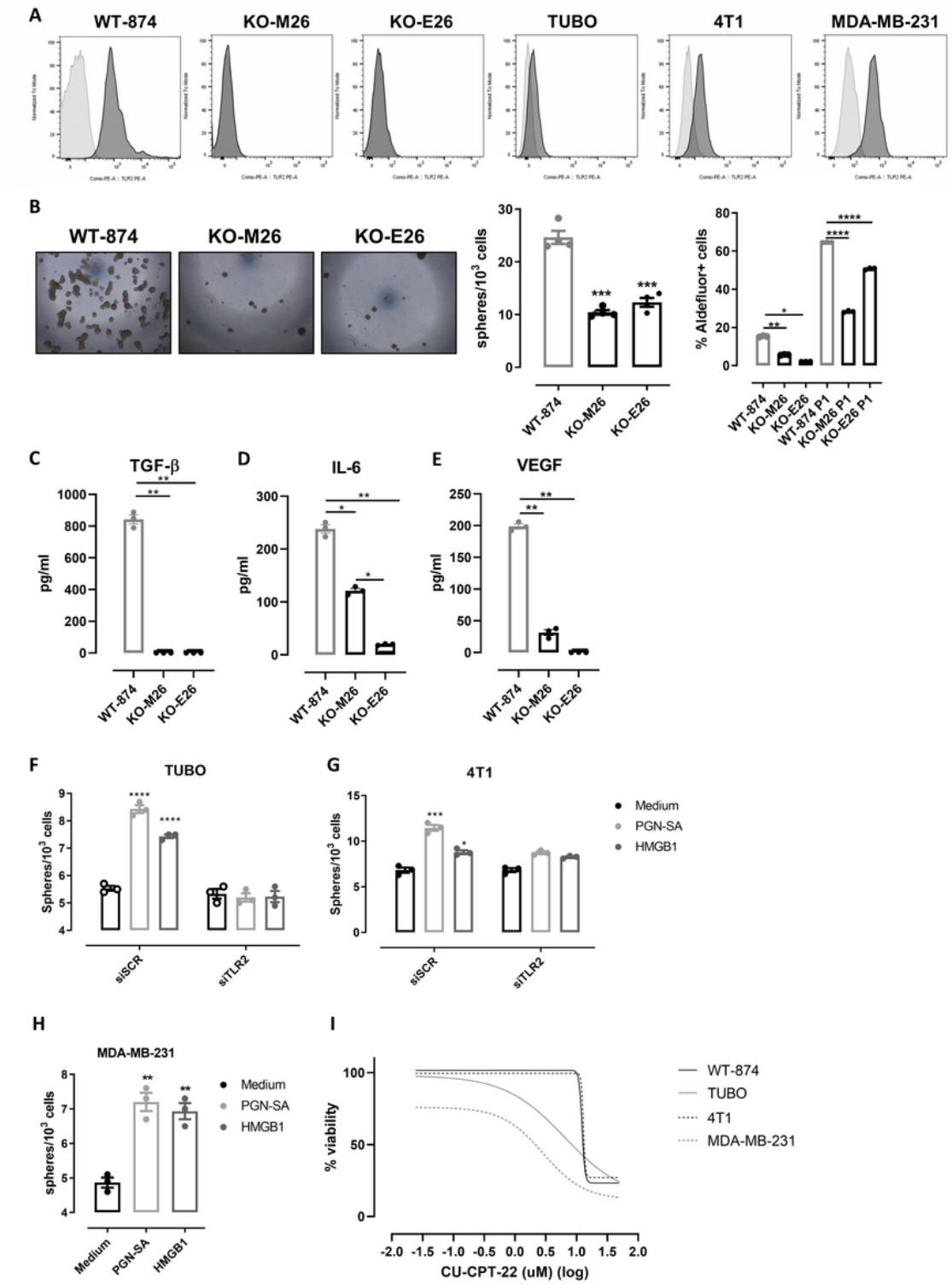

Figure 4

TLR2 promotes breast CSC self-renewal and its inhibition impairs cell viability. (A) Representative FACS histograms of TLR2 (dark gray) and control (light gray) staining on WT-874, KO-M26, KO-E26, TUBO, 4T1 and MDA-MB-231 cells. (B) Representative images of tumorspheres (Magnification 10X), sphere-generating ability (number of tumorspheres generated every 103 plated cells), and means ± SEM of the percentage of Aldefluor+ cells in WT-874, KO-M26, and KO-E26 cells cultured for 5 days in 2D or tumorsphere-forming conditions. (C-E) ELISA of TGF-β, IL-6 and VEGF released into the supernatant of WT-874, KO-M26, KO-E26 cultured for 48 hours in 2D conditions (N = 3 independent experiments). (F, G) Tumorsphere-generating ability of TUBO and 4T1 cells transfected with a pool of scrambled siRNAs (siSCR) or siRNAs to TLR2 (siTLR2) treated, 24 hours after transfection, with PGN-SA or HMGB1 for 4 days. (H) Tumorsphere-generating ability of MDA-MB-231 cells treated with PGN-SA or HMGB1 for 5 days. (I) Concentration-dependent cytotoxicity of CU-CPT-22 (50 to 0.02 μM) on WT-874, TUBO, 4T1 and MDA-MB-231 cells, evaluated using MTT after 48 hours of treatment. The graph shows log(inhibitor) vs. response - variable slope (four parameters) non-linear regression of data from three independent experiments, calculated with GrapPad8 software. *, $P < 0.05$; **, $P < 0.01$, ***; $P < 0.001$; ****, $P < 0.0001$; Student's t-test.

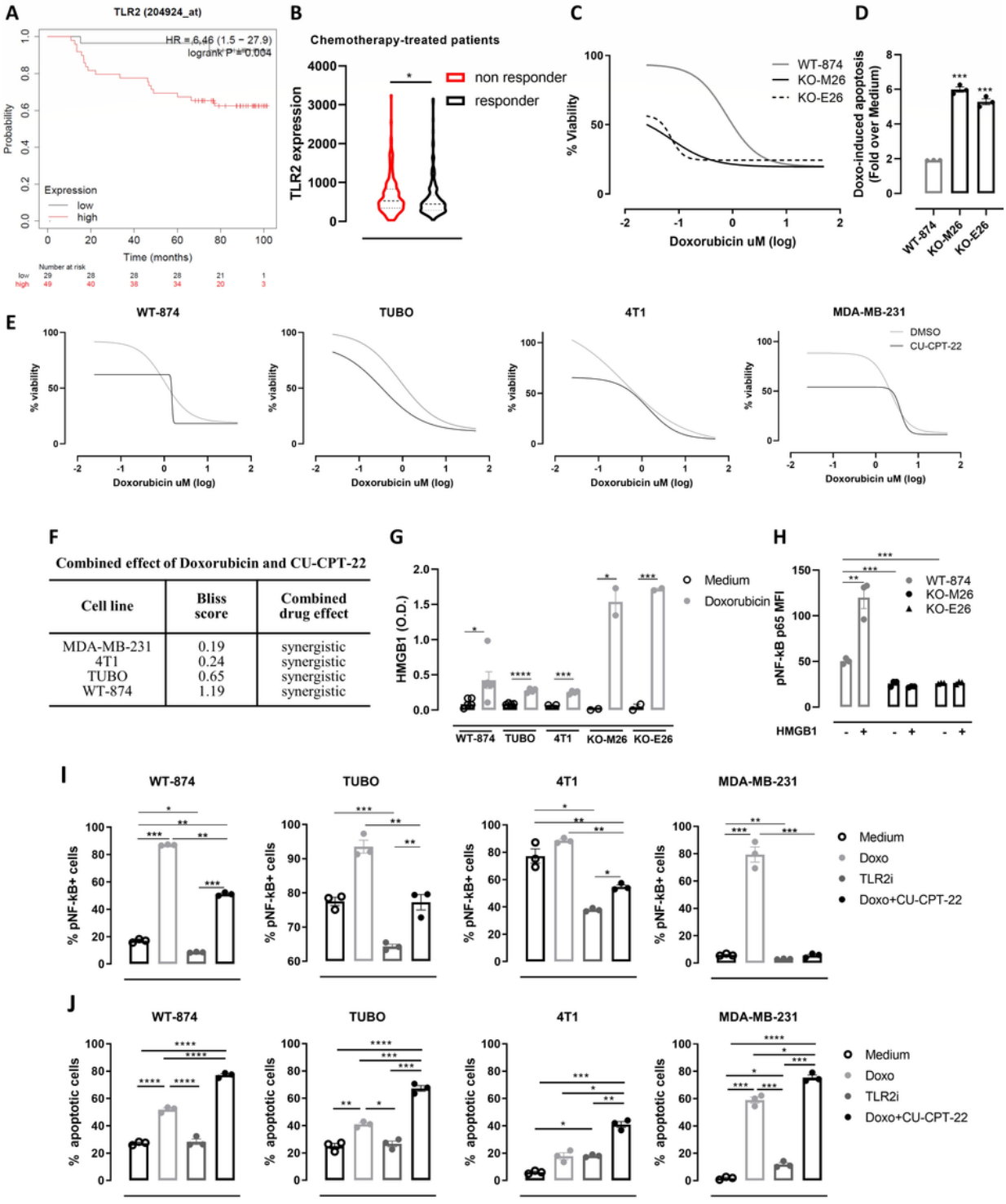

Figure 5

TLR2 promotes BC resistance to chemotherapy. (A) Kaplan–Meier plots displaying 5-year RFS of chemotherapy-treated BC patients stratified according to TLR2 mRNA expression (N = 78). (B) TLR2 mRNA expression levels in the tumors from BC patients that relapsed (Non-responders; N = 221) or not (responders; N = 256) within 5 years of adjuvant chemotherapy. (C) Concentration-dependent cytotoxicity of doxorubicin (50 to 0.02 μM) on WT-874, KO-M26 and KO-E26 cells, evaluated by MTT after 48 hours of

treatment. The graph shows log(inhibitor) vs. response - variable slope (four parameters) non-linear regression of data from three independent experiments, calculated using GrapPad8 software. (D) WT-874, KO-M26 and KO-E26 cells were treated with doxorubicin for 48 hours and analyzed using Annexin-V/propidium iodide FACS staining. The graph shows means ± SEM of the % of Annexin-V+ cells in doxorubicin-treated cells, as compared to the medium conditions, from three independent experiments. (E) Concentration-dependent cytotoxicity of doxorubicin (50 to 0.02 μM) alone or combined with 5 μM CU-CPT-22 on WT-874, TUBO, 4T1 and MDA-MB-231 cells, evaluated via MTT after 48 hours of treatment in three independent experiments. (F) Analysis of the effect of the combination of doxorubicin and CU-CPT-22 on BC cell lines. Bliss score > 0: synergistic effect; Bliss score = 0: additive effect; Bliss score < 0: antagonistic effect. (G) ELISA analysis of HMGB1 released into the supernatant by BC cells that were treated with doxorubicin for 48 hours or left untreated. The graph shows means ± SEM of HMGB1 concentration from ≥2 independent experiments. (H) FACS analysis of p65 NF-κB phosphorylation in WT-874, KO-M26 and KO-E26 cells treated with HMGB1 for 30 minutes or left untreated. The means ± SEM of mean fluorescence intensity (MFI) from three independent experiments are reported. (I, J) WT-874, TUBO, 4T1 and MDA-MB-231 cells were treated for 48 hours with or without doxorubicin, CU-CPT-22 or a combination of both. (I) Graphs of FACS analysis of p65 NF-κB phosphorylation. (J) Annexin-V/propidium iodide analysis of cell apoptosis. All graphs report the means ± SEM of the percentage of positive cells from three independent experiments. *, P < 0.05; **, P < 0.01; ***, P < 0.001; ****, P < 0.0001; Student’s t tests.

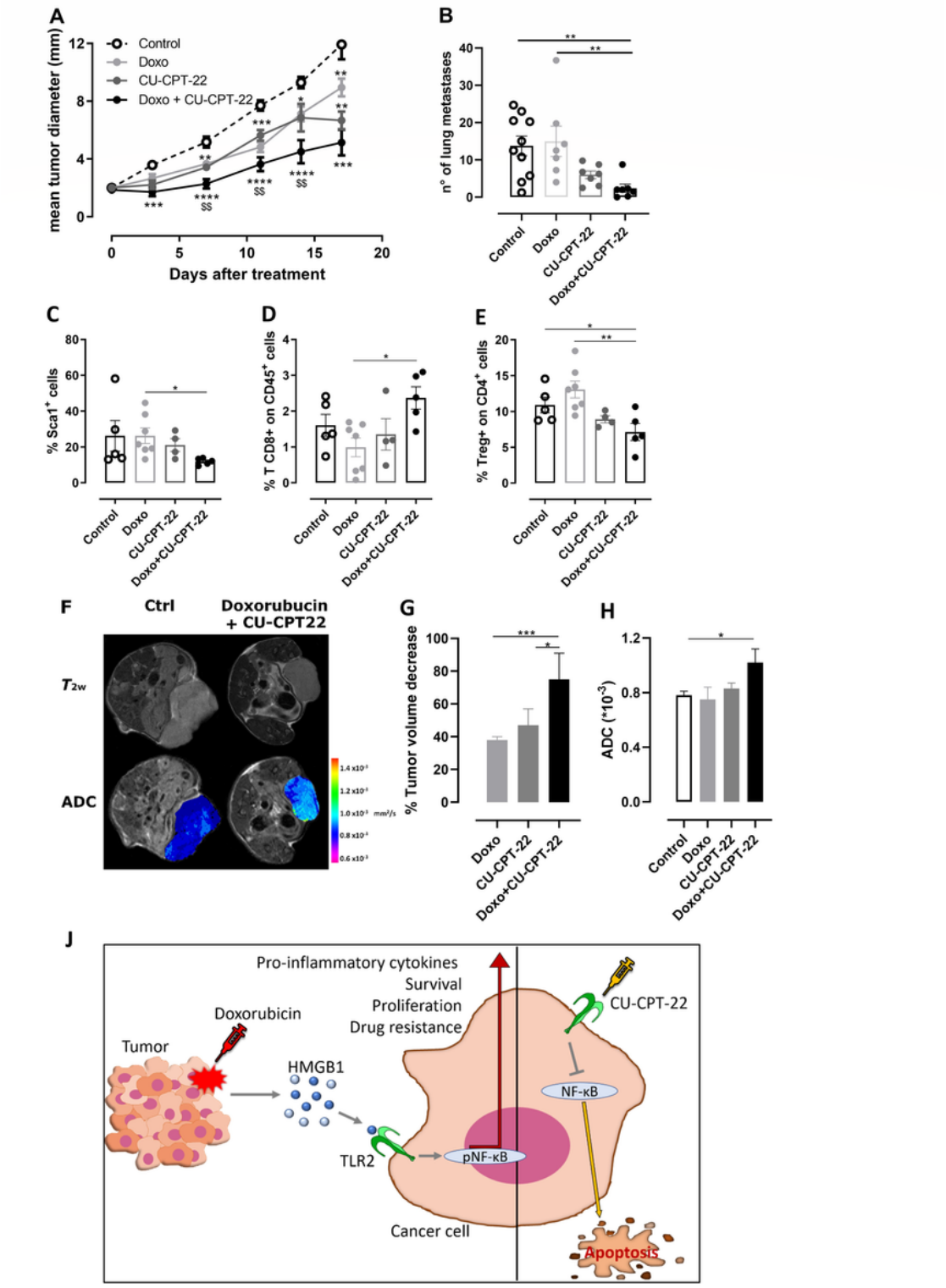

Figure 6

TLR2 inhibition synergizes with chemotherapy in impairing BC growth in-vivo. BALB/c mice were orthotopically challenged with 1x104 4T1 cells. When the tumors reached 2 mm in diameter, the mice were treated i.p. with 3 mg/kg doxorubicin and intratumorally with 50 µg CU-CPT-22, or the vehicle alone as a control (N = 7 per treated groups and N = 10 per control group). The treatment was repeated twice per week. Graphs show (A) mean tumor diameter, and (B) the number of spontaneous lung metastases

per square mm measured in lungs. FACS analysis of (C) Sca1+ cells from among CD45-, (D) CD8+ T cells from among CD45+ leucocytes and (E) Tregs from among CD4+ T cells in the tumors. Graphs show means ± SEM of the percentage of positive cells (N ≥ 4). Each circle represents a mouse. (F-H) T2w and DWI axial MR images of mice were acquired at the end point of the treatment. (F) Representative T2w axial images and false color representative axial ADC maps of the tumor region (superimposed on morphological T2w MR images) of control and doxorubicin + CU-CPT-22-treated mice. (G) Tumor volume was measured by manually drawing ROIs in the tumor for all axial slices covering the entire tumor (Fiji-ImageJ free software). Decrease of volume in the treated mice was reported as the percentage of the volume of control mice (mean ± SD). (H) Mean ± SD of ADC values from the tumors of treated mice. (J) Schematic representation of the mechanism of TLR2-dependent chemoresistance and of the effects of CU-CPT-22 treatment in combination with doxorubicin. *, P < 0.05; **, P < 0.01; ***; P < 0.001; ****, P < 0.0001; Student's t-test or (B) Mann-Whitney test. In (A), *: Doxo+CU-CPT-22, Doxo or CU-CPT-22 vs Control; $: Doxo + CU-CPT-22 vs Doxo and CU-CPT-22.

Supplementary Files

This is a list of supplementary files associated with this preprint. Click to download.

- Additionalfile1SupplementaryFig1.jpg
- Additionalfile2SupplementaryFig2.jpg
- Additionalfile3SupplementaryFig3.jpg
- Additionalfile4SupplementaryFig4.jpg
- Additionalfile5SupplementaryFig5.jpg
- Additionalfile6SupplementaryFig6.jpg
- Additionalfile7SupplementaryFig7.jpg